



Identification of clusters in multifocal electrophysiology recordings to maximize discriminant capacity (patients vs. control subjects)

M. Ortiz del Castillo · B. Cordón · E. M. Sánchez Morla · E. Vilades ·
M. J. Rodrigo · C. Cavaliere · L. Boquete · E. Garcia-Martin

Received: 1 June 2019 / Accepted: 4 September 2019 / Published online: 19 September 2019
© The Author(s) 2019

Abstract

Purpose To propose a new method of identifying clusters in multifocal electrophysiology (multifocal electroretinogram: mfERG; multifocal visual-evoked potential: mfVEP) that conserve the maximum capacity to discriminate between patients and control subjects.

Methods The theoretical framework proposed creates arbitrary N -size clusters of sectors. The capacity to discriminate between patients and control subjects is assessed by analysing the area under the receiver operator characteristic curve (AUC). As proof of concept, the method is validated using mfERG recordings taken from both eyes of control subjects ($n = 6$) and from patients with multiple sclerosis ($n = 15$).

Results Considering the amplitude of wave P1 as the analysis parameter, the maximum value of AUC = 0.7042 is obtained with $N = 9$ sectors. Taking into account the AUC of the amplitudes and latencies of waves N1 and P1, the maximum value of the AUC = 0.6917 with $N = 8$ clustered sectors. The greatest discriminant capacity is obtained by analysing the latency of wave P1: AUC = 0.8854 with a cluster of $N = 12$ sectors.

Conclusion This paper demonstrates the effectiveness of a method able to determine the arbitrary clustering of multifocal responses that possesses the greatest capacity to discriminate between control subjects and patients when applied to the visual field of mfERG or mfVEP recordings. The method may prove helpful in diagnosing any disease that is

M. O. del Castillo · C. Cavaliere · L. Boquete
Biomedical Engineering Group, Electronics Department,
University of Alcalá, Alcalá de Henares, Spain

B. Cordón · E. Vilades · M. J. Rodrigo ·
E. Garcia-Martin
Ophthalmology Department, Miguel Servet University
Hospital, Zaragoza, Spain

B. Cordón · E. Vilades · M. J. Rodrigo (✉) ·
E. Garcia-Martin
Aragon Institute for Health Research (IIS Aragon),
Miguel Servet Ophthalmology Innovation and Research
Group (GIMSO), University of Zaragoza,
50009 Zaragoza, Spain
e-mail: mariajesusrodrigo@hotmail.es

E. M. Sánchez Morla
12 de Octubre University Hospital Research Institute
(i + 12), Madrid, Spain

E. M. Sánchez Morla
Faculty of Medicine, Complutense University of Madrid,
Madrid, Spain

L. Boquete · E. Garcia-Martin
RETICS: Thematic Networks for Co-operative Research
in Health for Ocular Diseases, Barcelona, Spain

M. O. del Castillo
School of Physics, University of Melbourne, Melbourne,
VIC 3010, Australia

identifiable in patients' mfERG or mfVEP recordings and is extensible to other clinical tests, such as optical coherence tomography.

Keywords Multifocal electroretinogram · Multifocal visual-evoked potential · Multiple sclerosis · Visual field

Introduction

Multifocal visual-evoked potentials make it possible to obtain the individual responses produced in either the retina (multifocal electroretinogram: mfERG) or at cortical level (multifocal visual-evoked potential: mfVEP) by light excitation of a large number of sectors of the visual field (typically between 60 and 120).

The basic principles of the multifocal visual excitation technique are the result of research [1] into pseudorandom sequences conducted in the 1990s. Subsequent advances have facilitated its application in research and clinical environments [2].

These responses can be studied individually by sector, although the signal-to-noise ratio improves and the analysis time decreases if the responses are studied by cluster of sectors. Another advantage of the clustering approach is that it facilitates clinical topographic interpretation of the results.

The guidelines on mfERG [3] indicate the possibility of clustering the responses by quadrant, hemiretinal area, normal and abnormal regions of two eyes, or successive rings from centre to periphery. Responses from stimulus sectors associated with a local area of interest can be averaged for comparison with a similar area in an unaffected eye or with data from control subjects.

In a large number of publications, clustering by ring is used to analyse mfERG recordings, especially in diseases that produce altered responses with approximate radial symmetry. Examples include [4] (for diagnosis of glaucoma) and [5] (for identifying retinal toxicity due to treatment with hydroxychloroquine). Another study [6] concludes that using the central ring in mfERGs is an appropriately sensitive technique with which to study the progression of age-related macular degeneration over short periods of time.

Analysis by quadrant makes it possible to carry out comparisons between mfERG studies and optical coherence tomography (OCT) [7, 8]. It is also common to find the results of clustering by ring and quadrant in publications that analyse the technical aspects of mfERG [9, 10]. More recently, [11] detected altered responses in clustering by ring and quadrant in patients with nasopharyngeal carcinoma after radiotherapy.

Due to the irregular structure of the eye, which lacks symmetry of any kind, there is no basis for arguing that the predefined regions are in all cases those that possess the greatest capacity to discriminate between patients and control subjects. We therefore hypothesize that maximum affectionation by a particular disease can present in any cluster within the visual field and can have an arbitrary shape and size and may not necessarily present in rings, quadrants or hemispheres.

To date, guidelines for mfVEP procedures have not been published. Clustering of mfVEP responses in various eccentric rings makes it possible to identify patients with multiple sclerosis (MS) [12, 13]. Analysis of mfVEP responses in the inner (0.87° – 5.67°) and outer rings (5.68° – 24°) is proposed as a method for assessing optic nerve dysfunction in patients with optic disc drusen [14]. The best results achieved in implementing computer-aided diagnosis of multiple sclerosis are obtained by analysing the characteristics of the mfVEP responses when clustered by ring [15]. Clustering mfVEP responses in quadrants are useful in the study of amblyopic eyes [16] or for comparing OCT against mfVEP [17], [18].

The purpose of this paper is to propose a method of grouping the multifocal visual responses with the greatest capacity to discriminate between control subjects and patients affected by any disease identifiable in these responses. This grouping technique can be used for any pathology with neuroretinal or macular impact, and can be applied to various electrophysiological techniques (both in isolation and in combination).

This paper analyses mfERG signals in a comparative cohort of control subjects and patients affected by MS. Although MS is not an ophthalmological disease per se, eye function is very frequently affected. Moreover, as a neurodegenerative disease, MS-derived damage to the retinal nerve fibre layer (RNFL)

has been detected using OCT, reflecting the progressive axonal damage caused by the development of the disease which, in addition, has been linked to patient disability, even in those without a history of optic neuritis [19–21].

This paper also evaluates the diagnostic capacity of mfERG sector clustering, a technique that has been shown to be effective with mfVEP recordings.

Materials and methods

Patients and method

The system proposed may be used for any multifocal electrophysiology technique (e.g. mfERG or mfVEP) and for diagnosing any type of disease. In this paper, as proof of concept, the method may be useful to diagnose multiple sclerosis (MS) from mfERG recordings.

Subject database and mfERG acquisition

The study procedures were performed in accordance with the tenets of the Declaration of Helsinki, and ethical approval was obtained from the local ethics committee [Aragón Clinical Research Ethics Committee (CEICA, Zaragoza, Spain)]. All subjects were over the age of 18 and signed informed consent prior to study procedures.

The mfERG recordings from both eyes of 15 subjects (mean age 44.46 ± 8.24 , M:F = 4:11, $n = 30$ eyes) with newly diagnosed MS (less than 6 months) and no history of optic neuritis, and those from six control subjects (mean age 35.83 ± 10.65 , M:F = 3:3, $n = 12$ eyes), were used.

A complete neuro-ophthalmic examination was performed on all subjects in order to detect any ocular alteration that might affect functional vision or mfERG results. MS was diagnosed based on the 2010 revision of the McDonald Criteria [22]. The patients had no concomitant ocular diseases, nor any previous history of retinal pathology, glaucoma or significant refractive errors (more than 5 dioptres of spherical equivalent refraction or 3 dioptres of astigmatism), strabism or systemic conditions that could affect the visual system.

The mfERGs were recorded using the RETI-port/scan 21 (Roland Consult, Berlin, Germany) visual

electrophysiology system, according to the ISCEV standard [3]. The stimulus array consisted of 61 sectors, arranged hexagonally, displayed at a 60-Hz frame rate. The luminance of each sector was independently alternated between black ($< 2 \text{ cd/m}^2$ of luminance) and white (200 cd/m^2 of luminance) according to a pseudorandom binary m -sequence. The active channels were recorded using Dawson–Trick–Litzkow (DTL) electrodes fabricated from a flexible, lightweight nylon wire impregnated with silver and placed in contact with the conjunctival sac. The electrodes were placed below the lower eyelid, with one end being attached to the external canthus and the other end being attached at the height of the conjunctival sac. Three spoon electrodes were used, two as reference electrodes placed on each temple and the third as an earth electrode placed at the height of the nasion. An amplifier with 10^4 gain and 10–200 Hz bandwidth was used. The signals were digitized at a sample rate of 1017 samples/s, with the number of samples from each signal being 84 (82.61 ms long). The first-order mfERG kernel was analysed.

Before recording the mfERG signals, the characteristics of the test were explained to the subjects in order to achieve satisfactory fixation. During the test, both the acquisition device and the staff monitored the recordings to ensure that they were taken correctly. The recordings were examined by an expert ophthalmologist to identify potential issues relating to eccentric fixation, among others, before conducting a blind analysis of the signals.

Clustering

The method proposed requires the following inputs:

- A database of multifocal recordings taken from patients (MS) and control subjects.
- Definition of one or more parameters used to evaluate the capacity to discriminate between patients and control subjects. For mfERG records, potential parameters could be wave amplitude (A_{N1}, A_{P1}), latencies (L_{N1}, L_{P1}) or other suitable parameters (for example, obtained from the signals' decomposition wavelet).
- In order to obtain a minimum signal-to-noise ratio value, each cluster is considered to comprise at least $N_{\text{MIN}} = 5$ sectors. The maximum number of

sectors in a possible cluster is equal to the number of sectors in the visual field: N_{MAX} .

- The capacity to discriminate between patients and control subjects is evaluated using the area under the receiver operator characteristic curve (AUC). The AUC can be taken from one of the parameters or from the mean value of several.

Definition of valid clusters

Given a value of N ($N_{MIN} = 5 \leq N \leq N_{MAX} = 61$), a cluster defined as valid contains N -contiguous sectors (i.e. all the sectors belonging to the cluster are adjacent to at least two others in the cluster). Figure 1a shows two valid clusters while Fig. 1b shows two invalid clusters. In both cases, $N = 7$.

All possible sector clusters were analysed as per the conditions described above, including conventional clustering by ring, with the exception of Ring 1, which comprises a single sector.

Implementation of the method

Drawing on the database of patients and control subjects, for every value of N ($N_{MIN} \leq N \leq N_{MAX}$): (i) the valid clusters are identified; (ii) the mean of the multifocal responses of the sectors that comprise the cluster is calculated; (iii) the parameter or parameters of interest are obtained from the mean signal; (iv) the AUC between patients and control subjects is calculated; and (v) if the value of the AUC is the highest obtained so far, its details (N value, cluster identification) are saved until the procedure is completed.

It is possible to analyse two or more of the recordings’ parameters. To do so, the value of the AUC must be obtained for each of them. For example, Eq. (1) shows the AUC for the mean value of the amplitudes; Eq. (2) shows the mean value of the AUC obtained in analysis of the latencies; and Eq. (3) shows the mean value of the joint analysis of those 4 parameters.

$$AUC_{AMP} = \frac{AUC_{A_{PI}} + AUC_{A_{NI}}}{2} \tag{1}$$

$$AUC_{LAT} = \frac{AUC_{L_{PI}} + AUC_{L_{NI}}}{2} \tag{2}$$

$$AUC_{MEDIA} = \frac{AUC_{A_{PI}} + AUC_{A_{NI}} + AUC_{L_{PI}} + AUC_{L_{NI}}}{4} \tag{3}$$

It would also be possible to apply a different weighting to the partial AUC values that make up the overall AUC. Equation (4) shows a hypothetical case in which the discriminant capacity of the latencies is prioritised over that of the amplitudes.

$$AUC_{GLOBAL} = 0.2 * AUC_{A_{PI}} + 0.2 * AUC_{A_{NI}} + 0.3 * AUC_{L_{PI}} + 0.3 * AUC_{L_{NI}} \tag{4}$$

The arranged hexagonal sectors of the mfERG response are codified with the system of coordinates (q, r) shown in Fig. 2. The central sector (number 31) has the coordinates ($q = 0, r = 0$). These coordinates are able to efficiently codify the six neighbouring sectors for every single hexagon (each hexagon has six equidistant neighbours). As example, q and r positive

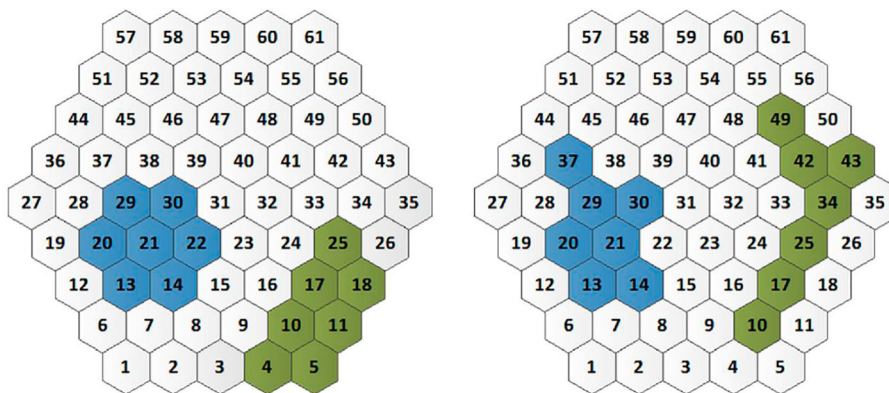


Fig. 1 Examples of possible clusters ($N = 7$). a Valid clusters. b Invalid clusters

values from Fig. 2 codify sectors nearly corresponding to the inferior nasal quadrant.

Figure 3 shows the flowchart of the method implemented. For all N values between N_{MIN} and N_{MAX} , a search is conducted for all N -size clusters, taking each of the 61 sectors (S_i) as a seed. In Step 1, the coordinates of the seed sector are obtained as per Fig. 2, while in Step 2, all the N -size clusters originating in sector S_i are obtained. The condition of Step 3 dictates that for every hexagon in the cluster analysed there must be at least two other hexagons at a distance equal to 1. The distance between two hexagons (H_1, H_2) in the system of coordinates proposed is calculated as follows:

$$D(H_1, H_2) = \frac{|q_1 - q_2| + |(q_1 + r_1) - (q_2 + r_2)| + |r_1 - r_2|}{2} \tag{5}$$

If the cluster fulfils the conditions, the signals of the sectors are averaged in both the control subjects and the patients and the value of the AUC (Step 4) is obtained until it is verified that all possibilities have been analysed (Step 5).

The number of clusters formed and analysed depends on the N -size. For example, for a value of $N = 5$, a total of 2 217 groups is analysed, while for a value of $N = 7$ the number of groups analysed rises to 26 224.

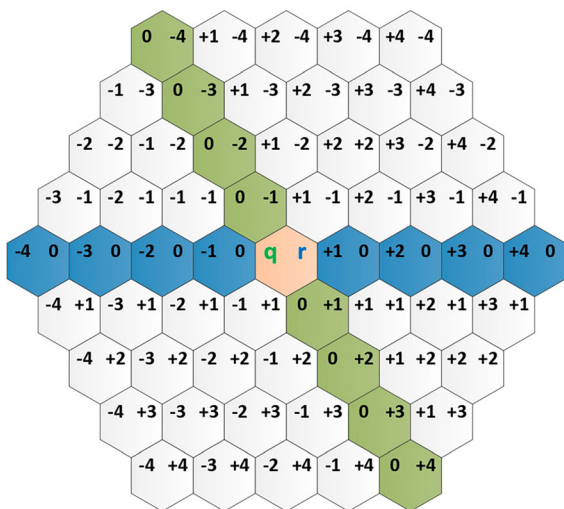


Fig. 2 System of coordinates used to find clusters

Results

Table 1 shows the AUC values obtained from conventional analysis by ring. Although clustering by ring (except Ring 1) is considered in cluster formation, these results make it possible to evaluate the advantages of the method proposed.

Figure 4 shows the clusters with greatest discriminant capacity ($N = 5 \dots N = 16$), considering the amplitude of wave P1 (A_{P1}) as the mfERG signal analysis parameter. The greatest discriminant value is obtained for $N = 9$ ($AUC_{(A_{P1}, N=9)} = 0.7042$), located in the inferior perifoveal quadrant (Rings 2, 3). For values of $N > 16$, the AUC values obtained continue to decrease.

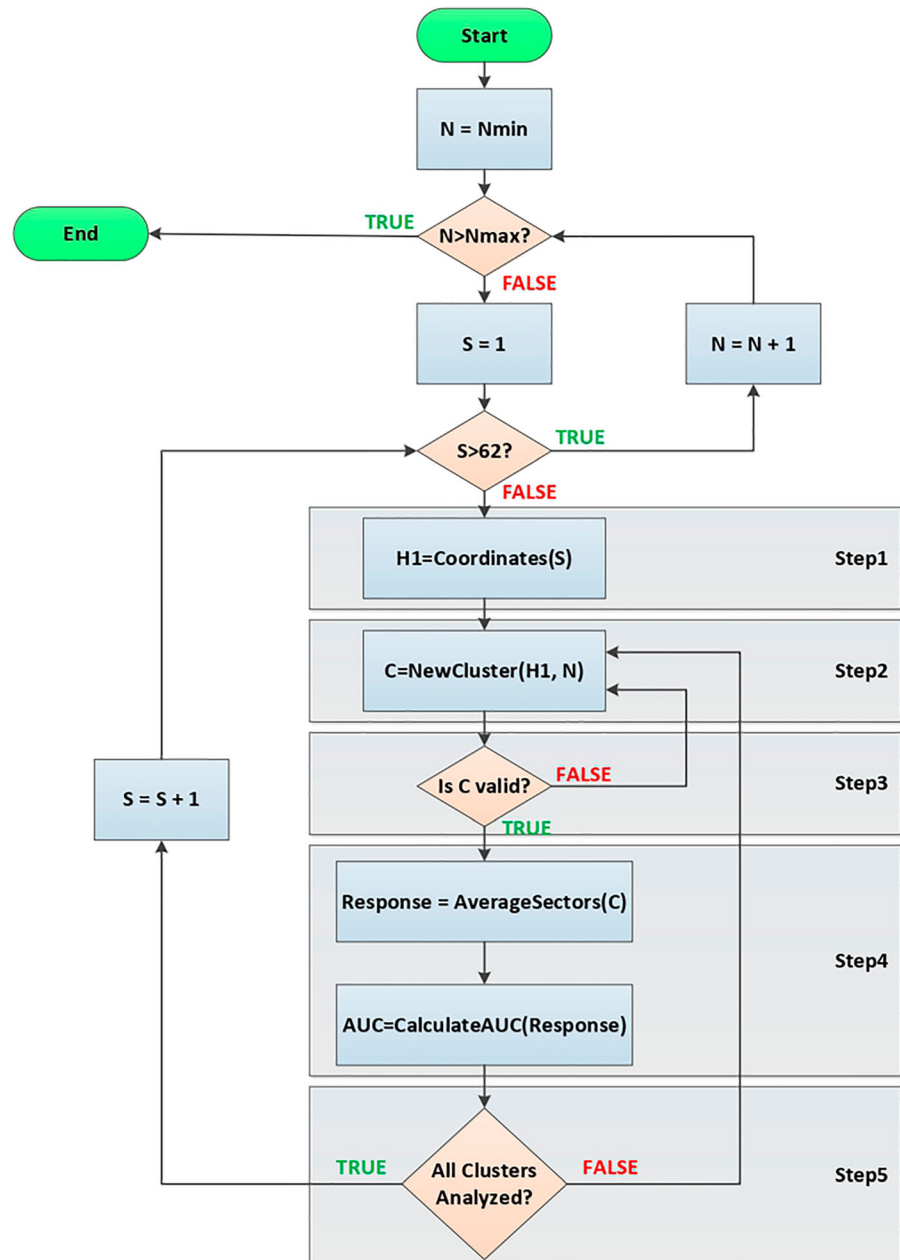
Figure 5 shows the results produced by several clusters, taking into account the four parameters (amplitudes and latencies of waves N1 and P1), and therefore, Eq. (3). According to this criterion, the maximum capacity to discriminate between patients with MS and control subjects is $AUC_{(A_{N1}, A_{P1}, L_{N1}, L_{P1}, N=8)} = 0.6917$. The AUC values obtained for $N > 16$ are less than 0.6917.

In recent publications, [10] and [23] observed that the latency of wave P1 is higher in MS patients. Figure 6 shows the results for this parameter, with the greatest discriminant capacity being $AUC_{(L_{P1}, N=12)} = 0.8854$, which corresponds to the nasal perifoveal area. In this case as well, clusters comprising more than 16 sectors do not obtain better AUC values.

Discussion

One of the advantages of the multifocal electrophysiology techniques is that they obtain a high number of responses in the visual field. However, in order to obtain a clear clinical interpretation of the results, it is necessary to apply clustering methods to the responses. Although studies usually group responses into predetermined shapes (rings and quadrants) and sizes (number of sectors) depending on the technique used and the disease to diagnose, it may be beneficial to identify clusters of arbitrary shapes and sizes. When analysing multifocal visual responses, it is very common to use pre-established cluster shapes (e.g. rings, quadrants or hemispheres). With our method, all

Fig. 3 Flowchart of the proposed method



possible options within the visual field are automatically and arbitrarily explored on the understanding that, for some signals and diseases, the optimal analysis areas do not necessarily coincide with pre-established clusters.

This article proposes an automatic method of selecting those areas of a topographic map of multifocal visual responses that present the greatest differences between patients and control subjects. The

method seeks the zone with greatest discriminant capacity, exceeding the AUC values obtained from clustering by ring (Table 1). Its efficacy in diagnosing MS from mfERG signals and using the amplitude and latency parameters of the first-order kernel responses to perform analysis has been demonstrated.

Among the options tested in our database, the highest AUC value is obtained by analysing the latency of wave P1 ($AUC_{(L_{P1}, N=12)} = 0.8854$); this

Table 1 AUC values obtained from analysis by ring

Region	Sectors	$AUC_{A_{P1}}$	$AUC_{\frac{A_{N1}+A_{P1}+L_{N1}+L_{P1}}{4}}$	$AUC_{L_{P1}}$
Ring 1	31	0.5958	0.5526	0.5771
Ring 2	22,23,30,32,39,40	0.5917	0.6115	0.6938
Ring 3	14,15,16,21,24,29,33,38,41,46,47,48	0.6417	0.5994	0.5854
Ring 4	7,8,9,10,13,17,20,25,28,34,37,42,45,49,52,53,54,55	0.5125	0.5328	0.5438
Ring 5	1,2,3,4,5,6,11,12,18,19,26,27,36,37,43,44,50,51,56,57,58,59,60,61	0.5708	0.6037	0.6896

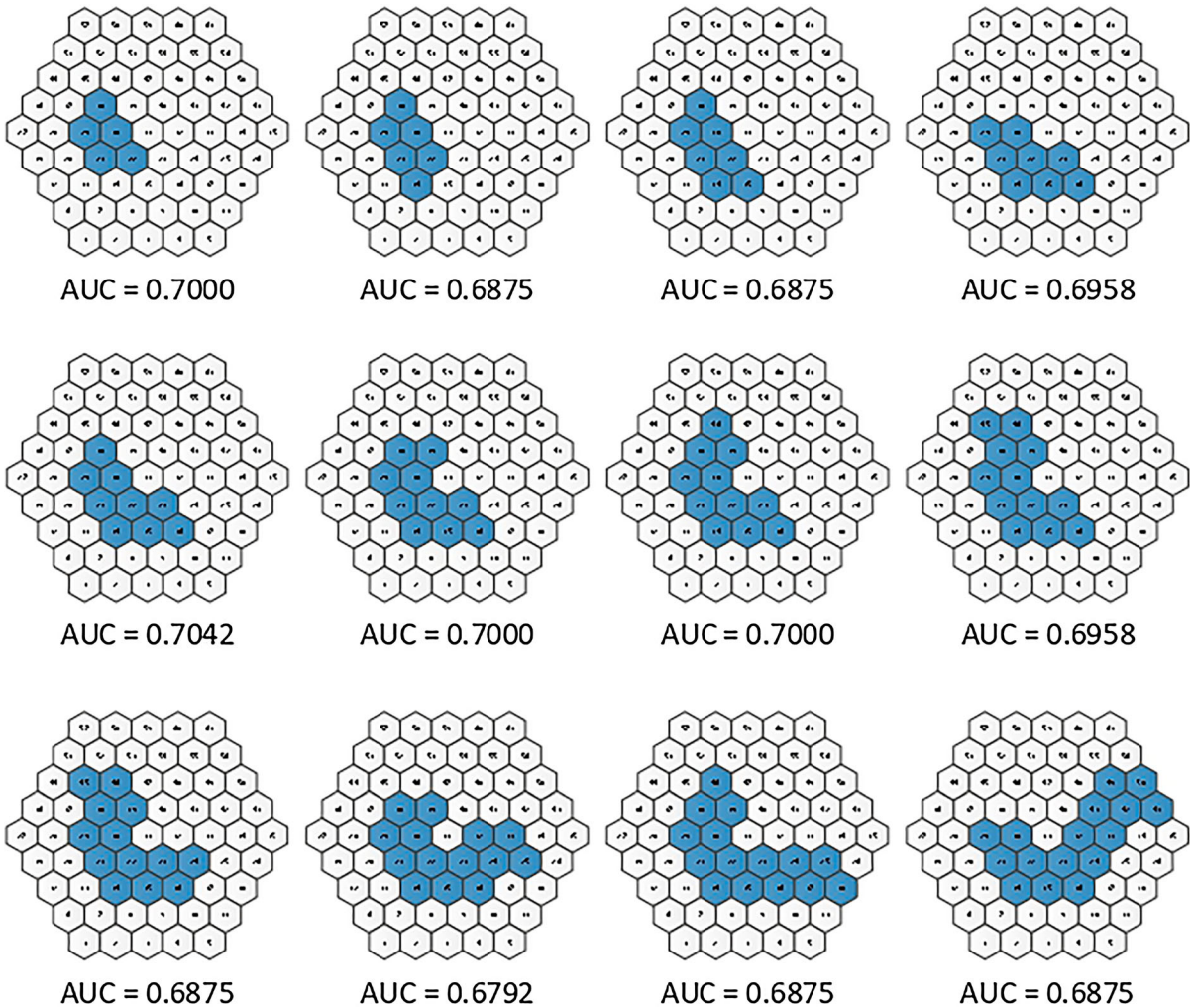


Fig. 4 Algorithm performance in selecting the best cluster for parameter A_{P1}

result is in agreement with [10] and [23]. Also, for our database, the highest AUC values were obtained by analysing clusters with fewer than 16 sectors.

The potential uses of the method proposed are listed below:

- With multifocal visual-evoked potentials, it can be used to analyse mfERG, mfVEP or mfPERG

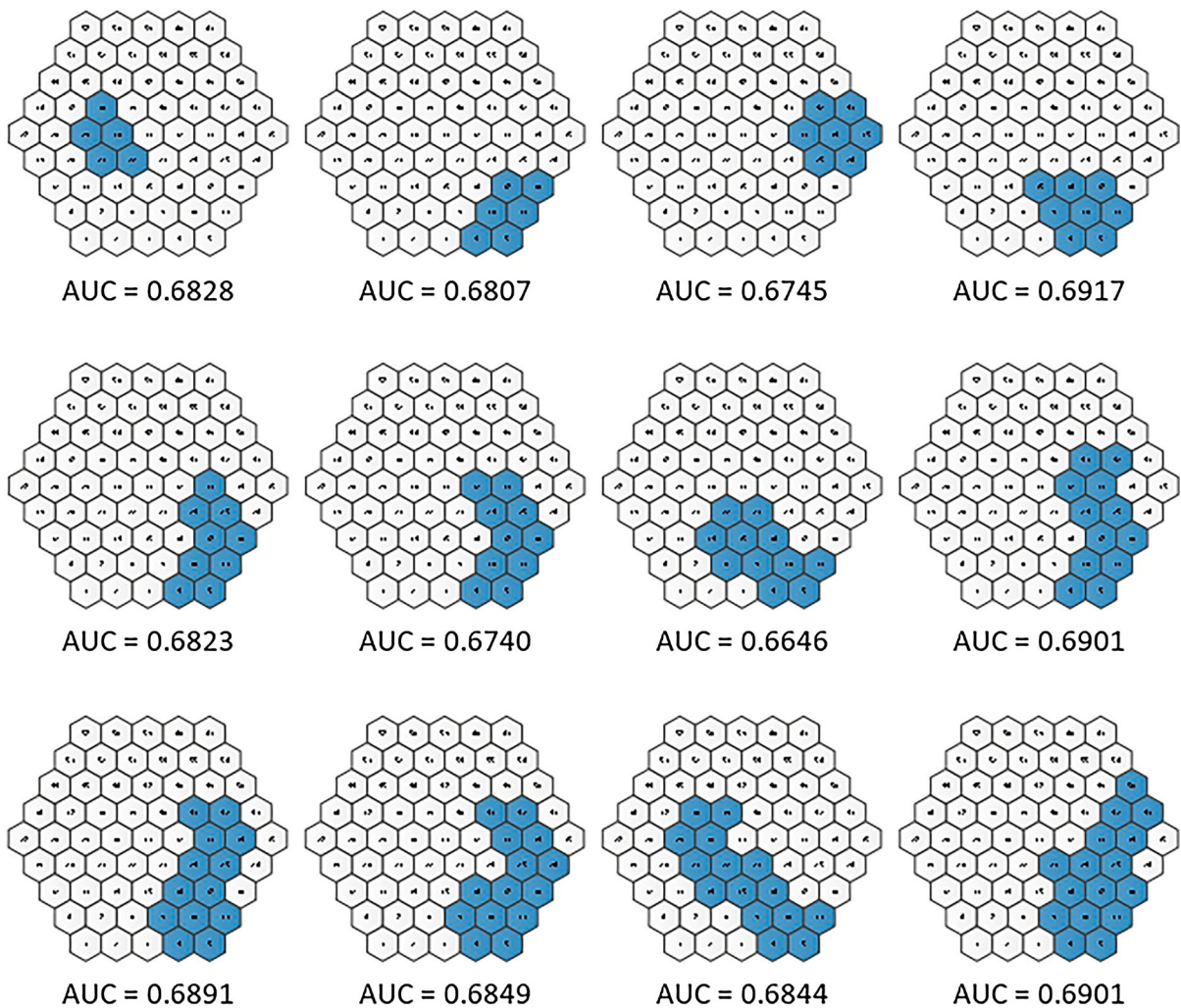


Fig. 5 Changes in the clusters, taking into account the maximum discriminant value for the mean of the two amplitudes and two latencies of waves N1 and P1

signals and can even be used to analyse areas of the automated perimetry. In general, it is applicable to any sector-based technique.

- The method is valid for any type of disease (MS, glaucoma, etc.) identifiable in these types of recordings.
- The AUC of one or several valid analysis parameters can be used. If the AUC is obtained from more than two parameters, each of them can be weighted with different coefficients.
- In studies of temporal evolution, the method can also be effective in detecting the region in which the most significant alterations appear.

It is also feasible to use it to analyse other types of tests, such as OCT. In line with this, [24] detects the retinal nerve fibre layer (RNFL) thicknesses found in angular sectors, which offer the best capacity for diagnosis in glaucoma patients.

With the method proposed in this paper it would be possible to determine which regions (of arbitrary shapes and sizes) are the most relevant for diagnosis. For example, with a Triton device with SS-OCT technology, it is possible to obtain grids of up to 60×45 points of measurement of the thickness of various layers of the retina. Detecting the areas

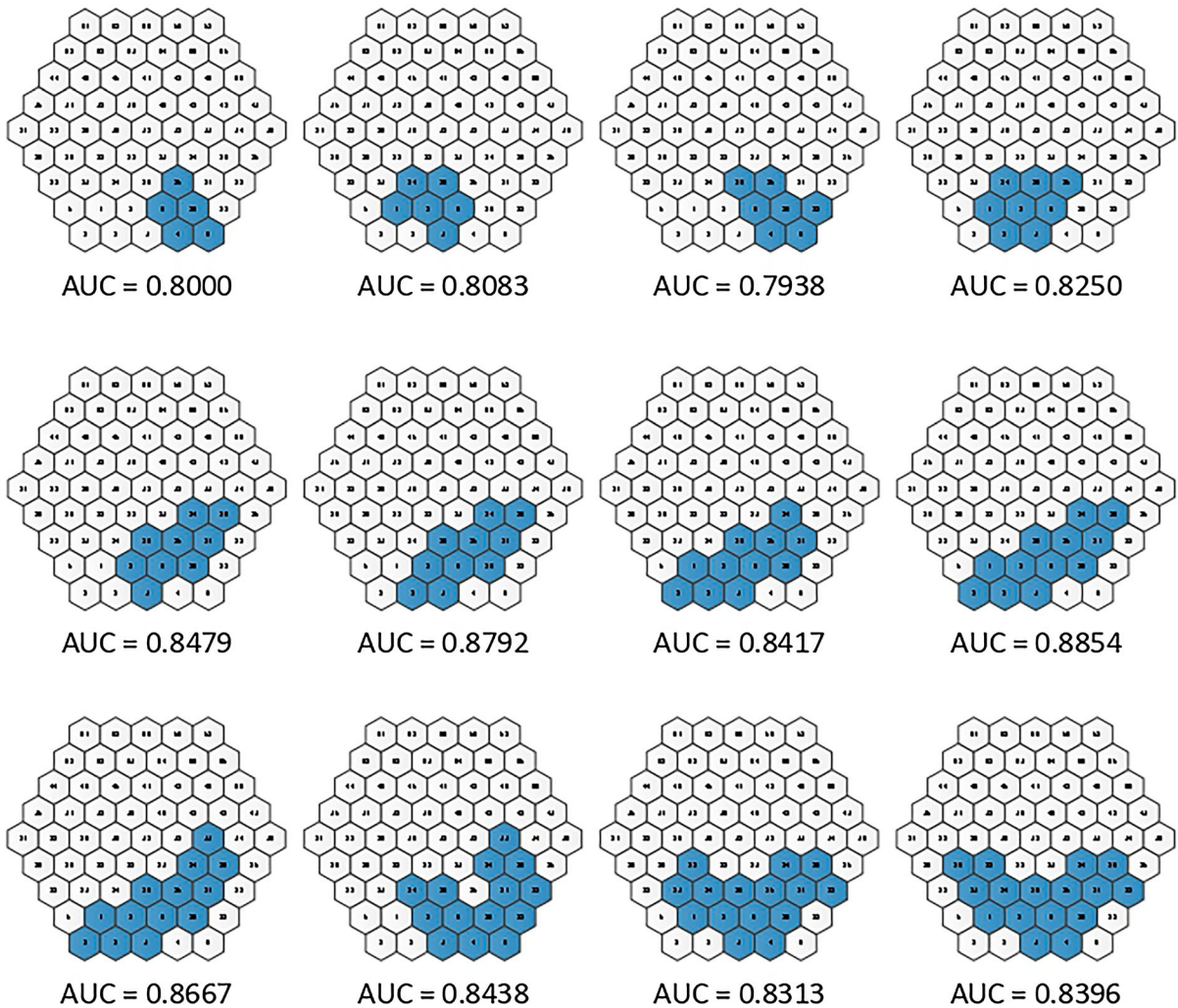


Fig. 6 AUC results for clusters identified using latency P1

suffering greatest alteration would be performed as follows:

- For one of the layers of the retina for which thickness measurements are available (e.g. RNFL), cells or basic sectors are formed. For example, if each cell comprises $5 * 5$ measurements, $N_{MAX} = 108$ sectors would be obtained.
- The mean value of the thickness in each of the sectors defined is then calculated.
- Starting from a minimum N value, a search is conducted for coherent cell clusters up to a maximum size of N_{MAX} . As the cells are square, it may be beneficial to consider that, to qualify as a valid cluster, all the cells should be adjacent to at least one other cell in the cluster. For each of the

valid clusters, the AUC is calculated and the algorithm selects the cluster and the N value with the highest AUC.

Our method found clusters that differentiated, with a high AUC, between patients with MS (as proof of concept) and healthy control subjects. However, because of the small size of our database, it is not possible to affirm that the clusters identified as having greatest discriminant capacity are specific to this disease. Our group considers it worthwhile to corroborate the results with further studies involving a higher number of patients and to compare them with other diseases. In such case, if it were possible to obtain a specific cluster for each disease, it would be possible to diagnose and monitor each of them individually. In

this regard, the clusters found in MS could be used as a valuable means of strengthening diagnosis or confirming non-definitive suspicions raised in earlier phases, such as when MRI does not reveal any damage.

In conclusion, this paper opens up the opportunity to identify sectors and clusters other than those arbitrarily chosen by the equipment manufacturer, basing them on the actual topographical affectation of a particular pathology at neuroretinal and cell level. This will enable better understanding of the physiopathological mechanisms of the diseases and expedite early diagnosis of them, which is the main objective of electrophysiological tests.

Acknowledgements This work was supported by the Carlos III Health Institute [Grant Number PI17/01726, “Neuro-ophthalmological evaluation as a biomarker of diagnosis, monitoring and prognosis in multiple sclerosis”, to EGM]; Secretary of State for Research, Development and Innovation [Grant Number DPI2017-88438-R (AEI/FEDER,UE) to LB] and RETICS Ofitared, RD16/0008/020 to RB and LB and RD16/0008/029 to EGM.

Funding This study was funded by Grants PI17/01726, DPI2017-88438-R, RD16/0008/020 and RD16/0008/029.

Data availability The datasets generated during and/or analysed during the current study are available from the corresponding author on reasonable request.

Compliance with ethical standards

Conflict of interest The authors declare that they have no conflict of interest.

Ethical approval All procedures performed in studies involving human participants were in accordance with the ethical standards of the institutional and/or national research committee [Aragón Clinical Research Ethics Committee (CEICA, Zaragoza, Spain)] and with the 1964 Helsinki declaration and its later amendments or comparable ethical standards.

Statement of human rights The study has been approved by local ethics committee [Aragón Clinical Research Ethics Committee (CEICA, Zaragoza, Spain), and it was conducted in accordance to the Helsinki Declaration.

Statement on the welfare of animals This article does not contain any studies with animals performed by any of the authors.

Informed consent Informed consent was obtained from all individual participants included in the study.

Open Access This article is distributed under the terms of the Creative Commons Attribution 4.0 International License (<http://creativecommons.org/licenses/by/4.0/>), which permits unrestricted use, distribution, and reproduction in any medium, provided you give appropriate credit to the original author(s) and the source, provide a link to the Creative Commons license, and indicate if changes were made.

References

1. Sutter EE (1991) The fast m-Transform: a fast computation of cross-correlations with binary m-Sequences. *SIAM J Comput* 20:686–694. <https://doi.org/10.1137/0220043>
2. Müller PL, Meigen T (2016) M-sequences in ophthalmic electrophysiology. *J Vis* 16:15. <https://doi.org/10.1167/16.1.15>
3. Hood DC, Bach M, Brigell M et al (2012) ISCEV standard for clinical multifocal electroretinography (mfERG) (2011 edition). *Doc Ophthalmol* 124:1–13. <https://doi.org/10.1007/s10633-011-9296-8>
4. Stiefelmeyer S, Neubauer AS, Berninger T et al (2004) The multifocal pattern electroretinogram in glaucoma. *Vis Res* 44:103–112. <https://doi.org/10.1016/j.visres.2003.08.012>
5. Arndt C, Costantini M, Chiquet C et al (2018) Comparison between multifocal ERG and C-Scan SD-OCT (“en face” OCT) in patients with a suspicion of antimalarial retinal toxicity: preliminary results. *Doc Ophthalmol* 136:97–111. <https://doi.org/10.1007/s10633-018-9625-2>
6. González-García E, Vilela C, Navea A et al (2016) Electrophysiological and clinical tests in dry age-related macular degeneration follow-up: differences between mfERG and OCT. *Doc Ophthalmol* 133:31–39. <https://doi.org/10.1007/s10633-016-9545-y>
7. Cascavilla ML, Parisi V, Triolo G et al (2018) Retinal dysfunction characterizes subtypes of dominant optic atrophy. *Acta Ophthalmol* 96:e156–e163. <https://doi.org/10.1111/aos.13557>
8. de Araújo RB, Oyama MK, Zacharias LC et al (2017) Morphological and functional inner and outer retinal layer abnormalities in eyes with permanent temporal hemianopia from chiasmal compression. *Front Neurol* 8:619. <https://doi.org/10.3389/fneur.2017.00619>
9. García-García Á, Muñoz-Negrete FJ, Rebolleda G (2016) Variability of the multifocal electroretinogram based on the type and position of the electrode. *Doc Ophthalmol* 133:99–108. <https://doi.org/10.1007/s10633-016-9560-z>
10. Neroev VV, Eliseeva EK, Zueva MV et al (2016) Demyelinating optic neuritis: optical coherence tomography and multifocal electroretinography data correlation. *Hum Physiol* 42:879–884. <https://doi.org/10.1134/S0362119716080090>
11. Gong H, Tang Y, Xiao J et al (2019) Evaluation of early changes of macular function and morphology by multifocal electroretinograms in patients with nasopharyngeal carcinoma after radiotherapy. *Doc Ophthalmol* 138:137–145. <https://doi.org/10.1007/s10633-019-09678-7>
12. Laron M, Cheng H, Zhang B, Frishman LJ (2009) The effect of eccentricity on the contrast response function of

- multifocal visual evoked potentials (mfVEPs). *Vis Res* 49:1711–1716. <https://doi.org/10.1016/j.visres.2009.03.021>
13. De Santiago L, Ortiz del Castillo M, Blanco R et al (2016) A signal-to-noise-ratio-based analysis of multifocal visual-evoked potentials in multiple sclerosis risk assessment. *Clin Neurophysiol* 127:1574–1580. <https://doi.org/10.1016/j.clinph.2015.09.129>
 14. Malmqvist L, de Santiago L, Boquete L, Hamann S (2017) Multifocal visual evoked potentials for quantifying optic nerve dysfunction in patients with optic disc drusen. *Acta Ophthalmol* 95:357–362. <https://doi.org/10.1111/aos.13347>
 15. de Santiago L, Sánchez Morla EM, Ortiz M et al (2019) A computer-aided diagnosis of multiple sclerosis based on mfVEP recordings. *PLoS ONE* 14:e0214662. <https://doi.org/10.1371/journal.pone.0214662>
 16. Jang J, Kyung SE (2018) Assessing amblyopia treatment using multifocal visual evoked potentials. *BMC Ophthalmol* 18:196. <https://doi.org/10.1186/s12886-018-0877-0>
 17. Qiao N, Zhang Y, Ye Z et al (2015) Comparison of multifocal visual evoked potential, static automated perimetry, and optical coherence tomography findings for assessing visual pathways in patients with pituitary adenomas. *Pituitary* 18:598–603. <https://doi.org/10.1007/s11102-014-0613-6>
 18. Sousa RM, Oyamada MK, Cunha LP, Monteiro MLR (2017) Multifocal visual evoked potential in eyes with temporal hemianopia from chiasmal compression: correlation with standard automated perimetry and OCT findings. *Invest Ophthalmol Vis Sci* 58:4436–4449. <https://doi.org/10.1167/iovs.17-21529>
 19. Zaveri MS, Conger A, Salter A et al (2008) Retinal imaging by laser polarimetry and optical coherence tomography evidence of axonal degeneration in multiple sclerosis. *Arch Neurol* 65:924–928. <https://doi.org/10.1001/archneur.65.7.924>
 20. Ayhan Z, Yaman A (2018) What does optical coherence tomography offer for evaluating physical disability in patients with multiple sclerosis? *Noro Psikiyatrs Ars* 55:S37–S40. <https://doi.org/10.29399/npa.23327>
 21. Garcia-Martin E, Ara JR, Martin J et al (2017) Retinal and optic nerve degeneration in patients with multiple sclerosis followed up for 5 years. *Ophthalmology* 124:688–696. <https://doi.org/10.1016/j.ophtha.2017.01.005>
 22. Polman CH, Reingold SC, Banwell B et al (2011) Diagnostic criteria for multiple sclerosis: 2010 revisions to the McDonald criteria. *Ann Neurol* 69:292–302. <https://doi.org/10.1002/ana.22366>
 23. Hanson JVM, Hediger M, Manogaran P et al (2018) Outer retinal dysfunction in the absence of structural abnormalities in multiple sclerosis. *Investig Ophthalmol Vis Sci* 59:549. <https://doi.org/10.1167/iovs.17-22821>
 24. Larrosa JM, Polo V, Ferreras A et al (2015) Neural network analysis of different segmentation strategies of nerve fiber layer assessment for glaucoma diagnosis. *J Glaucoma* 24:672–678. <https://doi.org/10.1097/IJG.0000000000000071>

Publisher's Note Springer Nature remains neutral with regard to jurisdictional claims in published maps and institutional affiliations.